nanomaterials

MDPI

Article

Tunable Electronic Properties of Type-II SiS_2/WSe_2 Hetero-Bilayers

Yue Guan [1,†], Xiaodan Li [1,*,†], Ruixia Niu [1], Ningxia Zhang [1], Taotao Hu [2] and Liyao Zhang [1]

[1] College of Science, University of Shanghai for Science and Technology, Shanghai 200093, China; 182282018@st.usst.edu.cn (Y.G.); 182282006@st.usst.edu.cn (R.N.); 182282021@st.usst.edu.cn (N.Z.); lyzhang@usst.edu.cn (L.Z.)

[2] School of Physics, Northeast Normal University, Changchun 130024, China; hutt262@nenu.edu.cn

* Correspondence: xiaodan_li@usst.edu.cn

† These authors contributed equally to this work.

Received: 25 September 2020; Accepted: 13 October 2020; Published: 15 October 2020

Abstract: First-principle calculations based on the density functional theory (DFT) are implemented to study the structural and electronic properties of the SiS_2/WSe_2 hetero-bilayers. It is found that the AB-2 stacking model is most stable among all the six SiS_2/WSe_2 heterostructures considered in this work. The AB-2 stacking SiS_2/WSe_2 hetero-bilayer possesses a type-II band alignment with a narrow indirect band gap (0.154 eV and 0.738 eV obtained by GGA-PBE and HSE06, respectively), which can effectively separate the photogenerated electron–hole pairs and prevent the recombination of the electron–hole pairs. Our results revealed that the band gap can be tuned effectively within the range of elastic deformation (biaxial strain range from −7% to 7%) while maintaining the type-II band alignment. Furthermore, due to the effective regulation of interlayer charge transfer, the band gap along with the band offset of the SiS_2/WSe_2 heterostructure can also be modulated effectively by applying a vertical external electric field. Our results offer interesting alternatives for the engineering of two-dimensional material-based optoelectronic nanodevices.

Keywords: first principle; hetero-bilayer; type-II band alignment; tunable band gap

1. Introduction

In the past two decades, the emergence of two-dimensional layered materials [1–4] has attracted tremendous attention of researchers due to their novel electronic properties, such as high carrier mobility [5,6], high thermal conductivity [7] and excellent on/off ratio [8], which ensure their potential application prospects in the field of photoemission, photodetection and field effect transistors (FETs). However, under the growing demands of material multifunction, the electronic properties of one single 2D material are far from enough [9,10]. For example, graphene, silicene and germanene, as the most promising materials, all have linear dispersion at the Fermi level at the K-point in the Brillouin zone. To our knowledge, one of the key factors for the development of 2D materials is dependent on its tunable band gap [11,12]. Thus, being a gapless semiconductor, graphene, silicene and germanene cannot be directly used in electronic optoelectronic devices [13,14]. However, if we introduce a hetero-bilayer system by stacking two single-layer materials vertically, the tunable band gaps could be realized by employing in-plane biaxial stress or changing the interlayer distance [15–18].

Recently, the heterostructures based on transition metal dichalcogenides (TMDs) [19,20], especially the WSe_2 [21–23] material, have attracted extensive research due to their excellent electronic and optoelectronic properties [24,25]. For example, Ren et al. established several TMDs-based van der Waals heterostructures (MoS_2/BP, $MoSe_2$/BP, WS_2/BP and WSe_2/BP) with bandgaps of 1.29, 1.37, 1.22 and 1.21 eV, respectively. Among them, $MoSe_2$/BP and WSe_2/BP possess type-II band alignment

with a direct band gap, which can separate the photogenerated electron–hole pairs effectively [26]. Engin Torun et al. predicted the existence of interlayer excitons (0.15 and 0.24 eV below the absorption onset of intralayer excitons) in MoS_2/WS_2 and $MoSe_2/WSe_2$ heterostructures, indicating that the excitonic ground states of these systems spontaneously separate the electron and the hole in different layers [27]. Si et al. also investigated the photoelectronic properties of MoS_2/WSe_2 heterojunction via the combination of theoretical prediction and experimental verification. They deduced that the enhancement of the photoelectric response should be attributed to the construction of the MoS_2/WSe_2 type-II heterostructure, which not only promotes the photogenerated electron–hole pair separation, but also suppresses their recombination [28]. Aretouli et al. found that $SnSe_2/WSe_2$ heterostructure possesses a broken gap configuration, indicating that band-to-band tunneling through an ultrathin van der Waals gap can be switched on and off easily via applying a small bias across the interface, which implies promising applications in 2D-2D vertical TFETs [29]. Thus, the heterostructures not only provide a new way to enrich the novel properties of the system but also to well preserve the electronic properties of the original freestanding two single-layer 2D components [30–32].

In this study, we perform ab initio calculations to investigate the electronic properties of hetero-bilayers composed of WSe_2 monolayer and SiS_2 monolayer (a new group of VI-IV 2D material [33]). Six possible stacking models are considered here. The geometries, relative stabilities and band structures of the considered models are discussed. Our results show that the most stable SiS_2/WSe_2 hetero-bilayer possesses the type-II band alignment with a narrow band gap, which contributes to the separation of electron–hole pairs. Furthermore, by applying a certain range of biaxial strain and external electric field, the band gap of the SiS_2/WSe_2 hetero-bilayer can be effectively tuned while maintaining the type-II band alignment. Our calculations and analysis demonstrate that the SiS_2/WSe_2 heterostructure may become a promising candidate material in the application of photoelectric devices.

2. Computational Method

To systematically investigate the structural and electronic properties of SiS_2/WSe_2 heterobilayers, we performed all calculations using the Vienna ab initio simulation package (VASP 5.4.1., Vienna, Austria) based on density functional theory (DFT) with the plane-wave pseudopotential methods [34,35]. The generalized gradient approximation (GGA), with the Perdew–Burke–Ernzerhof (PBE) function, was employed to describe the exchange and correlation potential [36,37]. Additionally, the hybrid Heyd–Scuseria–Eenzerhof (HSE06, Houston, TX, USA) functional was also used to obtain a more accurate bandgap [38]. In consideration of the weak van der Waals (vdW) interactions in all calculations, we used the DFT-D2 method of Grimme to correct the long-range weak vdW interlayer interactions [39]. A plane-wave kinetic energy cutoff of 500eV was adopted. The Monkhorst–Pack K-points [40] were set to $35 \times 35 \times 1$. A large vacuum zone of 20 Å was used to make the interaction between two adjacent 2D sheets in the periodic arrangement (along the "z" axis) negligible. The structure relaxations were carried out until the change of the energy and the force was less than 10^{-5} and 10^{-2} eV/Å per atom, respectively.

To quantitatively characterize the stability of the heterostructure, the binding energy of SiS_2/WSe_2 is defined as: $E_b = E_{SiS_2/WSe_2} - \left(E_{SiS_2} + E_{WSe_2}\right)$, where E_{SiS_2/WSe_2}, E_{SiS_2} and E_{WSe_2} represent the total energies of the SiS_2/WSe_2 hetero-bilayer, free-standing SiS_2 monolayer and isolated WSe_2 monolayer, respectively. E_{SiS_2} is calculated by using a 1×1 unit cell of the SiS_2 monolayer, and E_{WSe_2} is calculated by using a 1×1 unit cell of the WSe_2 monolayer (i.e., the size of the unit cells are the same as the supercell of the hetero-bilayer). To evaluate the interlayer electronic property and behavior of the SiS_2/WSe_2 heterobilayer, we also calculated the work function, defined as $\phi = E_0 - E_F$, where E_0 and E_F are the energy of the stationary electron in the vacuum and the Fermi level, respectively.

3. Results and Discussion

3.1. Structural Features of the Monolayer SiS_2, WSe_2 and SiS_2/WSe_2 Hetero-Bilayer

Before investigating the SiS_2/WSe_2 hetero-bilayer systems, we first study the electronic properties of isolated monolayer SiS_2 and monolayer WSe_2 (the space group of monolayer SiS_2 and monolayer WSe_2 are P3m1 and P63/mmc, respectively). The corresponding optimized structures of monolayer SiS_2 and monolayer WSe_2 are shown in Figure 1a,b. As shown in Figure 1, both of them have the same primitive cell of hexagonal structure with three atoms per unit cell. The lattice constants of SiS_2 and WSe_2 monolayers are calculated to be 3.30 and 3.33 Å, respectively, which agree well with previous results [33,41,42]. Compared with the hybrid systems investigated previously [21–32], such a lattice mismatch (only about 0.9%) between the SiS_2 and WSe_2 monolayers is very small. Thus, we have employed supercells composed of 1×1 unit cells of SiS_2 monolayer and 1×1 unit cells of WSe_2 monolayer in the x-y plane. To explore the possible stacking models of hetero-bilayers, we build six different stacking patterns of SiS_2/WSe_2 hetero-bilayers (labeled as AA-1, AA-2; AB-1, AB-2; AC-1, AC-2), as expressed in Figure 1c–h.

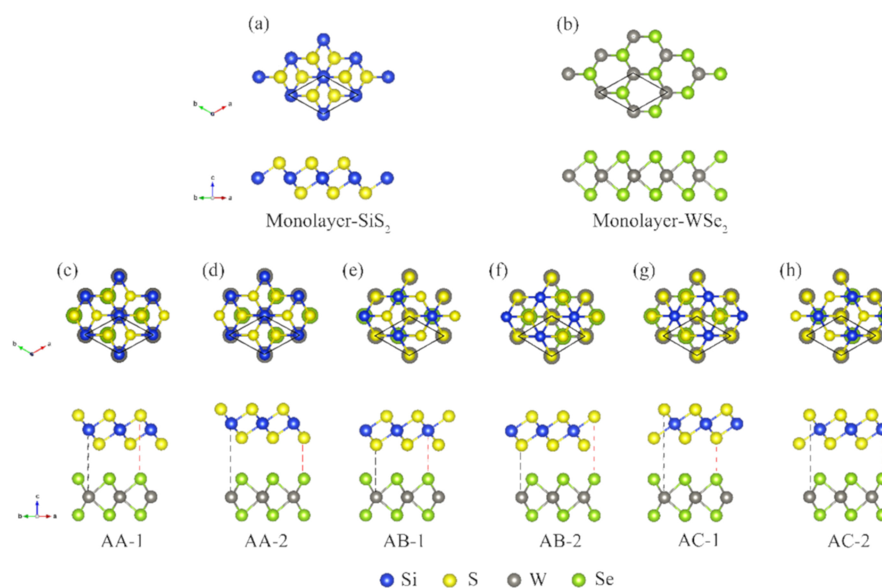

Figure 1. Top and side views of (**a**) monolayer SiS_2, (**b**) monolayer WSe_2 and (**c**–**h**) SiS_2/WSe_2 hetero-bilayers.

For AA-1 stacking, W atoms and Se atoms are located directly under the Si atoms and S (top sub-plane) atoms, respectively. For AB-1 stacking, W atoms and Se atoms are positioned just below the S atoms (bottom sub-plane) and Si atoms, respectively. For AC-1 stacking, W atoms and Se atoms are both positioned directly below the S atoms (top sub-plane and bottom sub-plane). The AA-2 (AB-2, AC-2) configuration is achieved by fixing the top layer of SiS_2 and rotating the WSe_2 layer of AA-1 (AB-1, AC-1) by 180 degrees with the "c" axis. The calculated binding energies for those configurations are shown in Table 1. According to our results, the binding energy of the AB-2 stacking (−197 meV) is shown to be larger than the binding energies of the other stacking models, indicating that the AB-2 model is the most stable and has the strongest bonding. These binding energies have the same order of magnitude as other typical vdW heterostructures such as the WSe_2/BP heterostructure (−141 meV) [26] and the $MoSe_2/MoS_2$ heterostructure (−158.1 meV) [43]. In addition to the binding energy, we also investigated the bond length, the interlayer spacing (the distance between the sulfur layer of the SiS_2 monolayer and its nearest selenium layer) and the band gaps of the hetero-bilayer systems, as shown in Table 1. Clearly, the calculated differences of lattice constants (around 2.33 Å) and bond lengths (around 2.54 Å) of Si-S and W-Se between the six hetero-bilayer models are very small. However, due to the change in relative position of atoms between the two layers, the interlayer

spacings exhibit relatively larger deviations. As shown in Table 1, the AB-2 stacking configuration has the shortest interlayer distance, showing again the strongest bonding in the hetero-bilayer system. Among all six of the SiS_2/WSe_2 hetero-bilayers, at the PBE level, the AB-2 stacking model is the only semiconductor. Since the AB-2 stacking model is the most stable stacking pattern, we now further discuss the electronic structures of the AB-2 stacking hetero-bilayer.

Table 1. The optimized structural parameters of SiS_2/WSe_2 heterostructures with different configurations, including the binding energy (E_b), lattice constant (a), bond length (d_{Si-S}, d_{W-Se}), the interlayer spacing (s), and the band gap (Eg) of the system obtained by GGA-PBE and hybrid HSE06.

Stacking Mode	E_b(meV)	a (Å)	$d_{Si\text{-}S}$(Å)	$d_{W\text{-}Se}$(Å)	s (Å)	E_g^{PBE}(eV)	E_g^{HSE06}(eV)
AA-1	−182.5	3.315	2.325	2.541	3.192	metal	/
AA-2	−125.1	3.315	2.326	2.542	3.784	metal	/
AB-1	−194.2	3.315	2.325	2.540	3.144	metal	/
AB-2	−197.0	3.315	2.324	2.541	3.125	0.154	0.738
AC-1	−125.0	3.314	2.325	2.541	3.788	metal	/
AC-2	−175.0	3.317	2.325	2.542	3.234	metal	/

3.2. Electronic Properties of the SiS_2/WSe_2 Hetero-Bilayer

Figure 2a,b demonstrates the band structures of monolayer SiS_2 and monolayer WSe_2 obtained by the GGA-PBE (black solid lines) and HSE06 (red dashed lines) method. It is clear that the pristine SiS_2 monolayer displays an indirect band gap semiconductor. The band gaps of monolayer SiS_2 obtained by the GGA-PBE and HSE06 method are 1.39 and 2.34 eV, respectively. Its valence-band maximum (VBM) is located between the high symmetry points Γ and M and the conduction-band minimum (CBM) is at the high symmetry M-point. In regard to the isolated monolayer WSe_2, it possesses a direct band gap of 1.48 eV (PBE level) or 2.0 eV (HSE06 level) at the high symmetric K-point. These results are consistent with previous studies [33,44,45]. After the 2D materials were constructed into hetero-bilayers, the band gaps narrowed or even disappeared. However, the electronic properties of origin SiS_2 and WSe_2 monolayers were well preserved. As mentioned above, at PBE level, the AB-2 stacking is the most stable configuration and it is the only semiconductor among the six configurations. For the AB-2 stacking configuration, as shown in Figure 2c, the CBM and VBM of the SiS_2 layer are both lower than those of the WSe_2, which forms a staggered type-II indirect band alignment. To further the discussion of the electronic structures of the SiS_2/WSe_2 hetero-bilayer, we also investigate the density of states. The total density of states is demonstrated by the black line. The orbital occupancy of each atom is clearly demonstrated in the projected density of states (the state with a low orbital occupancy is not shown in the figure). It can be seen clearly that, near the VBM (from −1 to 0 eV), the occupied states are almost dominated by W atoms (*d* orbitals) and Se atoms (*p* orbitals). While the electronic states above the Fermi level are contributed by Si (*s* orbitals) and S atoms (*p* orbitals). These results again confirm the type II band alignment of the AB-2 SiS_2/WSe_2 hetero-bilayer, which can effectively separate the photogenerated holes and electrons [46–49]. Owing to the narrower band gap (0.154 and 0.738 eV obtained by GGA-PBE and HSE06, respectively), the electrons are more susceptible to being excited from VBM to CBM when the SiS_2/WSe_2 heterostructure is exposed to light [50].

On the other hand, we also calculate the effective mass of AB-2 stacking model based on the formula as follows:

$$m^* = \hbar\left(\partial^2 E(k) / \partial k^2\right)^{-1} \tag{1}$$

Here, $\hbar$ is Plank's constant, $E(k)$ is the energy of CBM or VBM, and k is the wave vector. The effective mass is a key parameter to measure the mobility of carriers. Under certain conditions, the mobility μ is inversely proportional to the effective mass m^*. Our results show that the electron effective mass m_n^* of CBM is 0.43 m_0 (m_0 represents the mass of a free-electron), and the hole effective mass m_p^* of VBM is 0.47 m_0. A relatively small effective mass means higher carrier mobility [51]. Moreover, due to

effectively separating electron–hole pairs of type-II band alignment, the lifetime of photogenerated carriers is remarkably extended.

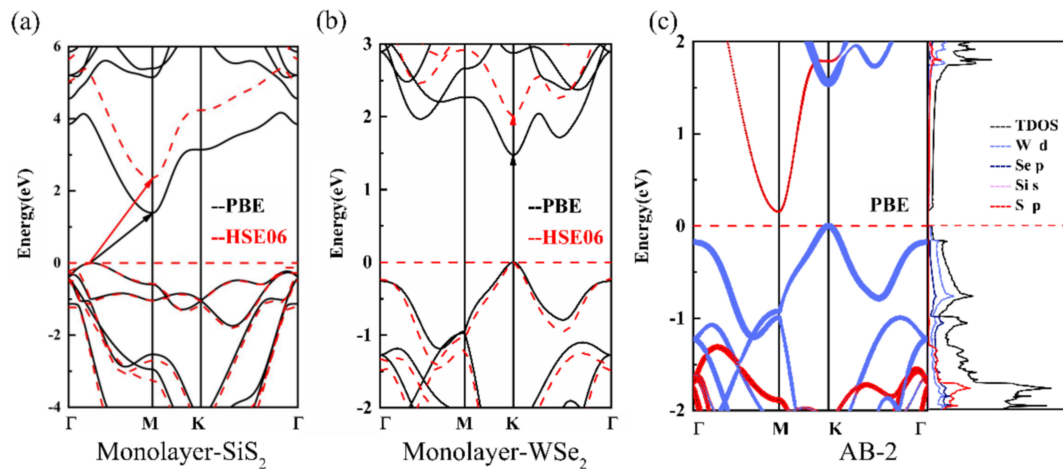

Figure 2. Energy band structures of (**a**) monolayer SiS_2 and (**b**) monolayer WSe_2. (**c**) Projected band structure and partial density of the state of AB-2 stacking SiS_2/WSe_2 hetero-bilayer; red and blue lines are bands contributed by SnS_2 and WSe_2 respectively.

The work function, which is crucial for evaluating the internal electronic behavior of heterostructures, is also discussed to explain the relevant charge transfer phenomenon (Figure 3a). The work functions of monolayer WSe_2 and monolayer SiS_2 are 5.15 and 6.49 eV respectively. Obviously, the work function of the WSe_2 sheet is smaller than that of the SiS_2 sheet, leading the electrons to spontaneously diffuse from WSe_2 to the SiS_2 layer in the SiS_2/WSe_2 hetero-bilayer. After the interaction between atomic layers, the Fermi level of WSe_2 is further moved downward while the Fermi level of SiS_2 is moved upward and finally reaches the same level, which causes the work function of the hetero-bilayer to be 5.21 eV. The same behaviors can be found in the electrostatic potential of the SiS_2/WSe_2 hetero-bilayer shown in Figure 3b. Due to the higher potential energy of WSe_2, the positive charges are accumulated in the WSe_2 layer, while the negative charges are accumulated in the SiS_2 layer. A built-in electric field directed from WSe_2 to SiS_2 is thus formed on the surface of the SiS_2/WSe_2 hetero-bilayer, resulting in a drift movement of the internal carriers. In addition, the calculated valence band offset (VBO) ΔE_V and conduction band offset (CBO) ΔE_C between the SiS_2 and WSe_2 layers reach 1.31 and 1.40 eV (1.33 and 1.66 eV) obtained by GGA-PBE (HSE06) method, respectively, as shown in Figure 3a. Such a huge band offsets can remarkably prolong the lifetime of interlayer carrier (electrons and holes) and improve the efficiency of carrier separation, which plays an indispensable role in the application of optoelectronic devices. Thus, most of the photogenerated electrons are transferred from the valence band of the WSe_2 layer to the conduction band of the SiS_2 layer. After a few photogenerated electrons jump to the conduction band of WSe_2 with higher energy, they will then transit to the conduction band of SiS_2 with lower energy. The photogenerated holes transfer process of the SiS_2/WSe_2 hetero-bilayer functions in an opposite manner.

In order to obtain a more accurate energy band gap, we also perform HSE06 calculations for the AB-2 stacking configuration, as shown in Figure 3c. The size of the red and blue dots respectively indicates the contribution of the SiS_2 layer and WSe_2 layer to the band structure. It is obvious that the the band at the CBM and VBM are contributed from the WSe_2 layer and the SiS_2 layer, respectively. The band gap of the SiS_2/WSe_2 hetero-bilayer, calculated by the HSE06 method, is 0.738 eV.

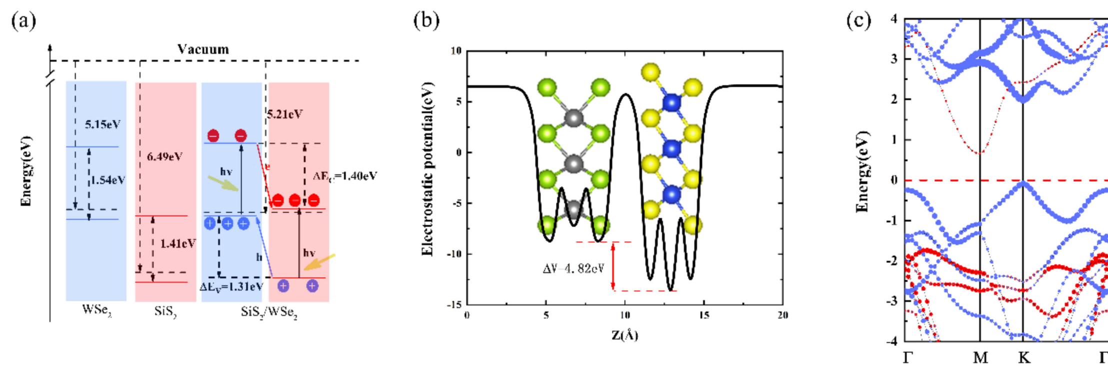

Figure 3. (**a**) Band alignment and (**b**) electrostatic potential of AB-2 SiS_2/WSe_2 hetero-bilayer obtained by GGA-PBE method. (**c**) Projected band structure of AB-2 SiS_2/WSe_2 hetero-bilayer obtained by the HSE06 method' red and blue lines are bands contributed by SnS_2 and WSe_2 respectively.

3.3. Effect of Biaxial Strain on Electronic Properties of SiS_2/WSe_2 Hetero-Bilayer

As is well known, strain modulation is an effective way to alter the electronic properties of 2D vdW heterostructures [52–54]. In this work, we applied the in-plane biaxial strain to the SiS_2/WSe_2 hetero-bilayer by changing the lattice constant of the system in both the x and y directions (i.e., compressive or tensile stresses). As shown in Figure 4a, blue and orange arrows represent the compressive and tensile strain, respectively. The degree of strain (ε) is defined as follows:

$$\varepsilon = \frac{a - a_0}{a_0} \times 100\% \quad (2)$$

where a and a_0 correspond to the strained and unstrained lattice constants of SiS_2/WSe_2 hetero-bilayer, respectively. Tensile (compressive) stress is represented by $\varepsilon > 0$ ($\varepsilon < 0$). The biaxial stresses range from −11% to 11% with an interval of 2%. To avoid the structure collapse of SiS_2/WSe_2 hetero-bilayer, we also calculate the strain energy E, which is defined as follows:

$$E = (E_{\text{total}} - E_0)/n \quad (3)$$

where E_{total} and E_0 represent the total energy of the strained system and the strain-free system, respectively. N is the number of atoms in the supercell. The results are shown in Figure 4b; the strain energy increases monotonously with increasing stress (compressive stresses: from 0 to −7%, tensile stresses: from 0 to 7%). Noteworthy is the evolution curve of the strain energy in this interval is close to the quadratic function of the strain, indicating that the stresses applied on the hetero-bilayer are within the elastic deformation limit. However, the strain energy curve begins to deviate from the original trend if the tensile (compressive) stress continues to increase, showing that the hetero-bilayer is undergoing inelastic deformation.

We also calculate the evolution curve of the band gap and band offsets of the SiS_2/WSe_2 hetero-bilayer as a function of the biaxial stress ε, as expressed in Figure 4c. In the range of elastic deformation (the stress changes from −7% to 7%), the band gap of the SiS_2/WSe_2 hetero-bilayer decreases gradually with increasing tensile stress. When the applied strain exceeds the range of elastic deformation, the change trend of energy band is opposite. In regard to the band offsets of the SiS_2/WSe_2 hetero-bilayer, the VBO increase continuously as the strain changes from −11% to 5%, then decreases with increasing tensile stress.

The change of band gap and band offsets of the SiS_2/WSe_2 hetero-bilayer can be intuitively shown in Figure 5, which is the projected band structure diagrams of the SiS_2/WSe_2 hetero-bilayer, obtained by the HSE06 method under different biaxial strains. The red and blue dotted lines indicate the contribution of SiS_2 and WSe_2, respectively. In the range of elastic deformation, the SiS_2/WSe_2 hetero-bilayer maintains its type-II band alignment with an indirect band gap. When the compressive stress reaches

−9%, the system turns into a direct band gap semiconductor with type-II band alignment. On the other hand, the SiS_2/WSe_2 hetero-bilayer system changed the band alignment from type-II to type-I when the tensile stress reaches 11%, which is attractive for realizing the nano-scale multi-functional device applications.

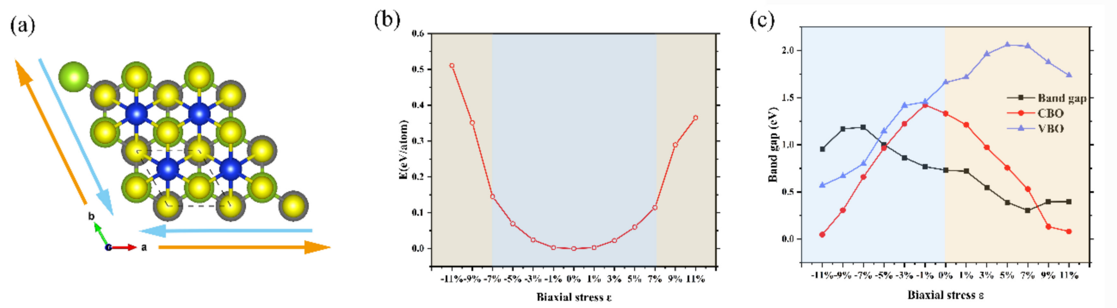

Figure 4. (**a**) Schematic diagram of tensile (orange arrows) and compressive (blue arrows) stresses on the SiS_2/WSe_2 hetero-bilayer. (**b**) Strain energy (E) as a function of strain of the biaxial stress ε. (**c**) Band gap and band offsets of the SiS_2/WSe_2 hetero-bilayer as a function of the biaxial stress ε.

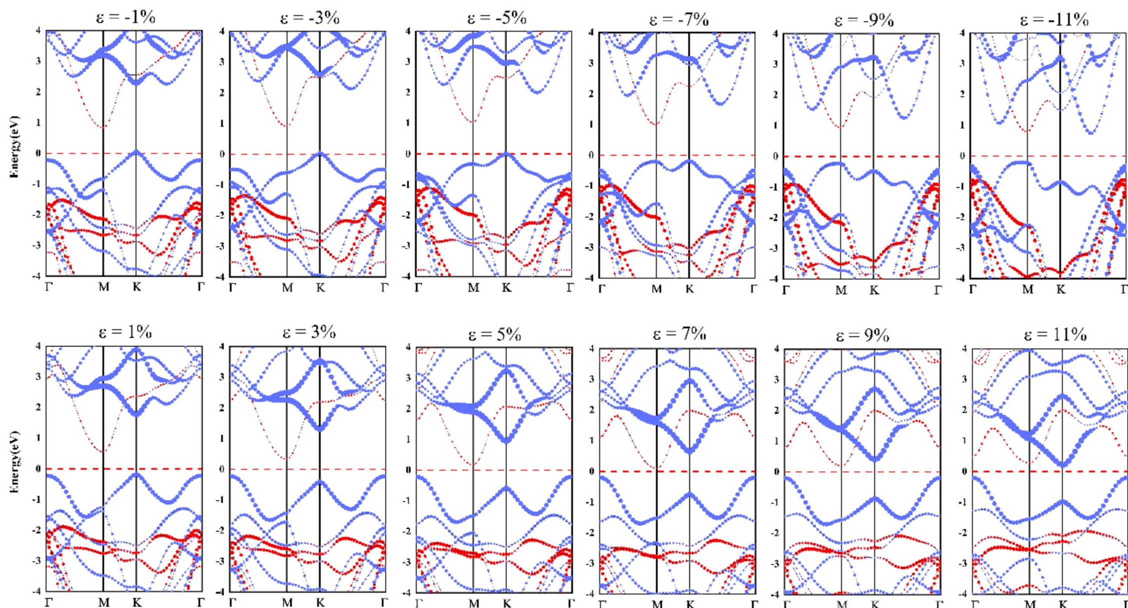

Figure 5. Projected band structures obtained by the HSE06 method under different in-plane biaxial stresses; red and blue lines are bands contributed by SnS_2 and WSe_2, respectively.

3.4. Effect of Electric Field on Electronic Properties of SiS_2/WSe_2 Hetero-Bilayer

Applying an external electric field (E_{ext}) has proven to be an effective method to tune the band gap [55,56]. In this section, we apply a vertical electric field (E_{ext}) along the z direction to the SiS_2/WSe_2 hetero-bilayer. The direction from the SiS_2 layer to the WSe_2 layer is defined as the positive direction of the E_{ext}, which is opposite to the direction of the E_{int} in the hetero-bilayer. The value of the band gap gradually increases with increasing negative E_{ext}, and reduces continuously with the increasing positive E_{ext}, as shown in Figure 6. The band gap as a function of the external electric field shows a trend of completely linear decrease, while the changes of VBO and CBO show a linear increase trend. The projected band structures of the SiS_2/WSe_2 hetero-bilayer under various E_{ext} are displayed in Figure 7. We find that the hetero-bilayer system could retain type-II band alignment features in the range of −0.1 V/Å to 0.5 V/Å for the external E-field, indicating that the E_{ext} has little influence on

the variations of the band structure of the systems. This is essential for the future application of the SiS_2/WSe_2 hetero-bilayer-based electronic devices, such as the field-effect transistor.

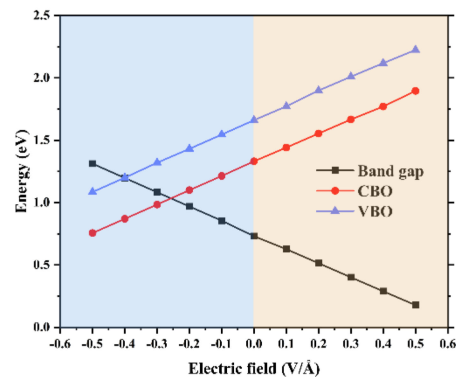

Figure 6. Band gap and band offsets of the SiS_2/WSe_2 hetero-bilayer as a function of the external electric field.

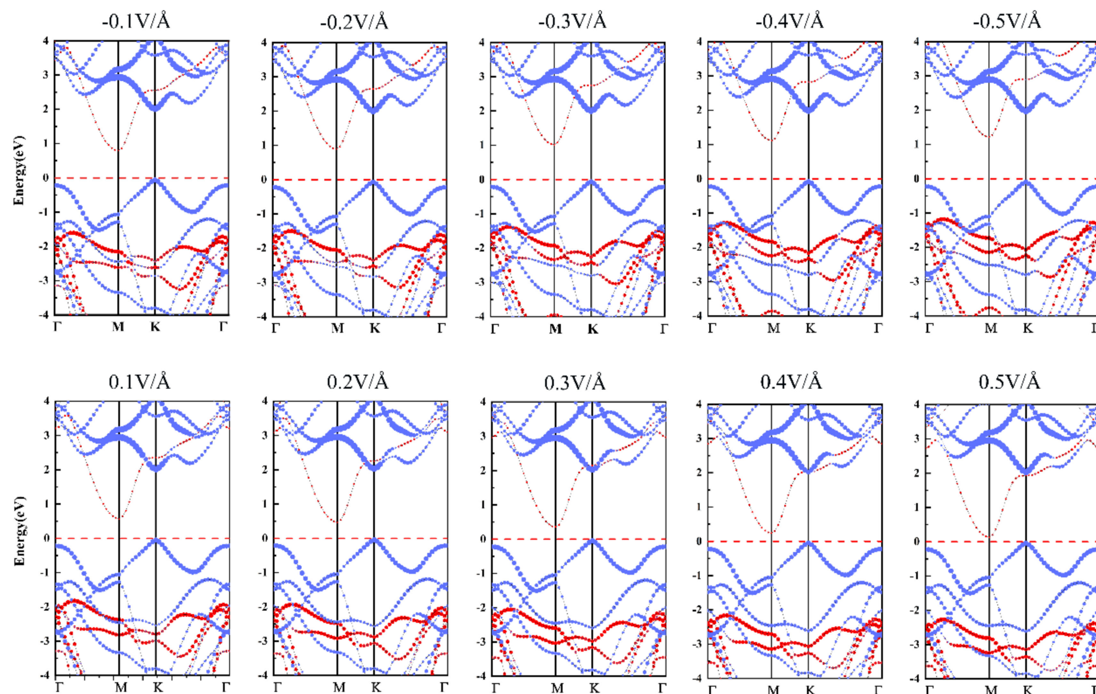

Figure 7. Projected band structures of the SiS_2/WSe_2 hetero-bilayers under different external electric fields obtained by the HSE06 method; red and blue lines are bands contributed by SnS_2 and WSe_2 respectively.

4. Conclusions

In summary, the structural and electronic properties of the SiS_2/WSe_2 hetero-bilayers are investigated in detail through first principles calculations. Our results show that the SiS_2/WSe_2 hetero-bilayer is an indirect band gap semiconductor (0.154 and 0.738 eV obtained by GGA-PBE and HSE06, respectively) with an intrinsic type-II band alignment. Meanwhile, the heterostructure perfectly retains the electronic properties of the pristine 2D monolayer components. Moreover, the SiS_2/WSe_2 hetero-bilayers have been shown to possess a relatively low effective mass, which enhances carrier mobility of the heterostructure. The type-II band alignment, narrow band gap, together with low effective mass conduce effective separation of photogenerated carriers, which is promising for application in optoelectronic devices. On the other hand, under biaxial strain, the heterostructure can withstand the biaxial strain from −7% (compressive) to 7% (tensile) while maintaining the type-II

band alignment. Moreover, through changing the effective electric field crossing the interface of the heterostructure, the band gap and band offset of the SiS_2/ WSe_2 hetero-bilayers can be effectively modulated by applying the external electric field. Our results offer promising alternatives for the engineering of two dimensional material-based optoelectronic nanodevices.

Author Contributions: Y.G.—writing, review, editing, writing original draft, conceptualization; X.L.—project administration, validation, resources, supervision, writing original draft, review and editing; R.N.—investigation, formal analysis; N.Z.—investigation, formal analysis; T.H.—investigation; L.Z.—investigation, editing. All authors have read and agreed to the published version of the manuscript.

Funding: This work is supported by the Fundamental Research Funds for the Central Universities, China under grant No. 2412019FZ037.

Conflicts of Interest: The authors declare no conflict of interest.

References

1. Novoselov, K.S.; Geim, A.K.; Morozov, S.V.; Jiang, D.; Zhang, Y.; Dubonos, S.V.; Grigorieva, I.V.; Firsov, A.A. Electric Field Effect in Atomically Thin Carbon Films. *Science* **2004**, *306*, 666–669. [CrossRef] [PubMed]
2. Bhimanapati, G.R.; Lin, Z.; Meunier, V.; Jung, Y.; Cha, J.; Schulman, D.S.; Xiao, D.; Son, Y.; Strano, M.S.; Cooper, V.R.; et al. Recent Advances in Two-Dimensional Materials beyond Graphene. *ACS Nano* **2015**, *9*, 11509–11539. [CrossRef] [PubMed]
3. Liu, H.; Neal, A.T.; Zhu, Z.; Luo, Z.; Xu, X.; Tománek, D.; Ye, P.D. Phosphorene: An Unexplored 2D Semiconductor with a High Hole Mobility. *ACS Nano* **2014**, *8*, 4033–4041. [CrossRef] [PubMed]
4. Tran, V.; Soklaski, R.; Liang, Y.; Yang, L. Layer-controlled band gap and anisotropic excitons in few-layer black phosphorus. *Phys. Rev. B* **2014**, *89*, 235319. [CrossRef]
5. Geim, A.K. Graphene: Status and Prospects. *Science* **2009**, *324*, 1530–1534. [CrossRef]
6. Ruppert, C.; Aslan, O.B.; Heinz, T.F. Optical Properties and Band Gap of Single- and Few-Layer MoTe2 Crystals. *Nano Lett.* **2014**, *14*, 6231–6236. [CrossRef]
7. Balandin, A.A.; Ghosh, S.; Bao, W.; Calizo, I.; Teweldebrhan, D.; Miao, F.; Lau, C.N. Superior Thermal Conductivity of Single-Layer Graphene. *Nano Lett.* **2008**, *8*, 902–907. [CrossRef]
8. Huang, L.; Huo, N.; Li, Y.; Chen, H.; Yang, J.; Wei, Z.; Li, J.; Li, S.-S. Electric-Field Tunable Band Offsets in Black Phosphorus and MoS_2 van der Waals p-n Heterostructure. *J. Phys. Chem. Lett.* **2015**, *6*, 2483–2488. [CrossRef]
9. Zhou, B.; Gong, S.-J.; Jiang, K.; Xu, L.; Shang, L.; Zhang, J.; Hu, Z.; Chu, J. A type-II GaSe/GeS heterobilayer with strain enhanced photovoltaic properties and external electric field effects. *J. Mater. Chem. C* **2020**, *8*, 89–97. [CrossRef]
10. Kumar, R.; Das, D.; Singh, A.K. C_2N/WS_2 van der Waals type-II heterostructure as a promising water splitting photocatalyst. *J. Catal.* **2018**, *359*, 143–150. [CrossRef]
11. Neto, A.H.C.; Guinea, F.; Peres, N.M.R.; Novoselov, K.S.; Geim, A.K. The electronic properties of graphene. *Rev. Mod. Phys.* **2009**, *81*, 109–162. [CrossRef]
12. Lui, C.H.; Mak, K.F.; Shan, J.; Heinz, T.F. Ultrafast Photoluminescence from Graphene. *Phys. Rev. Lett.* **2010**, *105*, 127404. [CrossRef]
13. Chen, X.; Yang, Q.; Meng, R.; Jiang, J.; Liang, Q.; Tan, C.; Sun, X. The electronic and optical properties of novel germanene and antimonene heterostructures. *J. Mater. Chem. C* **2016**, *4*, 5434–5441. [CrossRef]
14. Barhoumi, M.; Lazaar, K.; Said, M. DFT study of the electronic and vibrational properties of silicene/stanene heterobilayer. *Phys. E Low Dimens. Syst. Nanostruct.* **2019**, *111*, 127–129. [CrossRef]
15. Chiu, M.H.; Zhang, C.; Shiu, H.W.; Chuu, C.P.; Chen, C.H.; Chang, C.Y.; Chen, C.H.; Chou, M.Y.; Shih, C.K.; Li, L.J. Determination of band alignment in the single-layer MoS_2/WSe_2 heterojunction. *Nat. Commun.* **2015**, *6*, 7666. [CrossRef] [PubMed]
16. Xiong, W.; Xia, C.; Zhao, X.; Wang, T.; Jia, Y. Effects of strain and electric field on electronic structures and Schottky barrier in graphene and SnS hybrid heterostructures. *Carbon* **2016**, *109*, 737–746. [CrossRef]
17. Ghorbani-Asl, M.; Bristowe, P.D.; Koziol, K.; Heine, T.; Kuc, A. Effect of compression on the electronic, optical and transport properties of MoS_2/graphene-based junctions. *2D Mater.* **2016**, *3*, 025018. [CrossRef]

18. Wan, W.; Li, X.; Li, X.; Xu, B.; Zhan, L.; Zhao, Z.; Zhang, P.; Wu, S.Q.; Zhu, Z.-z.; Huang, H.; et al. Interlayer coupling of a direct van der Waals epitaxial MoS_2/graphene heterostructure. *RSC Adv.* **2016**, *6*, 323–330. [CrossRef]
19. Vu, T.V.; Hieu, N.V.; Phuc, H.V.; Bui, H.; Idrees, M.; Amin, B.; Hieu, N.N. Graphene/WSeTe van der Waals heterostructure: Controllable electronic properties and Schottky barrier via interlayer coupling and electric field. *Appl. Surf. Sci.* **2020**, *507*, 145036. [CrossRef]
20. Tongay, S.; Zhou, J.; Ataca, C.; Liu, J.; Kang, J.S.; Matthews, T.S.; You, L.; Li, J.; Grossman, J.C.; Wu, J. Broad-Range Modulation of Light Emission in Two-Dimensional Semiconductors by Molecular Physisorption Gating. *Nano Lett.* **2013**, *13*, 2831–2836. [CrossRef] [PubMed]
21. Rivera, P.; Schaibley, J.R.; Jones, A.M.; Ross, J.S.; Wu, S.; Aivazian, G.; Klement, P.; Seyler, K.; Clark, G.; Ghimire, N.J.; et al. Observation of long-lived interlayer excitons in monolayer $MoSe_2$–WSe_2 heterostructures. *Nat. Commun.* **2015**, *6*, 6242. [CrossRef]
22. Jin, C.; Regan, E.C.; Yan, A.; Iqbal Bakti Utama, M.; Wang, D.; Zhao, S.; Qin, Y.; Yang, S.; Zheng, Z.; Shi, S.; et al. Observation of moire excitons in WSe_2/WS_2 heterostructure superlattices. *Nature* **2019**, *567*, 76–80. [CrossRef]
23. Unuchek, D.; Ciarrocchi, A.; Avsar, A.; Watanabe, K.; Taniguchi, T.; Kis, A. Room-temperature electrical control of exciton flux in a van der Waals heterostructure. *Nat. Cell Biol.* **2018**, *560*, 340–344. [CrossRef]
24. Sun, M.; Chou, J.-P.; Yu, J.; Tang, W. Effects of structural imperfection on the electronic properties of graphene/WSe_2 heterostructures. *J. Mater. Chem. C* **2017**, *5*, 10383–10390. [CrossRef]
25. Kang, J.; Tongay, S.; Zhou, J.; Li, J.; Wu, J. Band offsets and heterostructures of two-dimensional semiconductors. *Appl. Phys. Lett.* **2013**, *102*, 012111. [CrossRef]
26. Ren, K.; Sun, M.; Luo, Y.; Wang, S.; Yu, J.; Tang, W. First-principle study of electronic and optical properties of two-dimensional materials-based heterostructures based on transition metal dichalcogenides and boron phosphide. *Appl. Surf. Sci.* **2019**, *476*, 70–75. [CrossRef]
27. Torun, E.; Miranda, H.P.C.; Molina-Sánchez, A.; Wirtz, L. Interlayer and intralayer excitons in MoS_2/WS_2 and $MoSe_2$/WSe_2 heterobilayers. *Phys. Rev. B* **2018**, *97*, 245427. [CrossRef]
28. Si, K.; Ma, J.; Lu, C.; Zhou, Y.; He, C.; Yang, D.; Wang, X.; Xu, X. A two-dimensional MoS_2/WSe_2 van der Waals heterostructure for enhanced photoelectric performance. *Appl. Surf. Sci.* **2020**, *507*. [CrossRef]
29. Aretouli, K.E.; Tsoutsou, D.; Tsipas, P.; Marquez-Velasco, J.; Aminalragia Giamini, S.; Kelaidis, N.; Psycharis, V.; Dimoulas, A. Epitaxial 2D $SnSe_2$/ 2D WSe_2 van der Waals Heterostructures. *ACS Appl. Mater. Interfaces* **2016**, *8*, 23222–23229. [CrossRef]
30. Nguyen, H.T.T.; Obeid, M.M.; Bafekry, A.; Idrees, M.; Vu, T.V.; Phuc, H.V.; Hieu, N.N.; Hoa, L.T.; Amin, B.; Nguyen, C.V. Interfacial characteristics, Schottky contact, and optical performance of a graphene/Ga_2SSe van der Waals heterostructure: Strain engineering and electric field tunability. *Phys. Rev. B* **2020**, *102*, 075414. [CrossRef]
31. Zeng, H.; Zhao, J.; Cheng, A.-Q.; Zhang, L.; He, Z.; Chen, R.-S. Tuning electronic and optical properties of arsenene/C_3N van der Waals heterostructure by vertical strain and external electric field. *Nanotechnology* **2018**, *29*, 075201. [CrossRef] [PubMed]
32. Li, X.D.; Wu, S.-Q.; Zhu, Z.-Z. Band gap control and transformation of monolayer-MoS_2 -based hetero-bilayers. *J. Mater. Chem. C* **2015**, *3*, 9403–9411. [CrossRef]
33. Naseri, M.; Abutalib, M.; Alkhambashi, M.; Gu, J.; Jalilian, J.; Farouk, A.; Batle, J. Prediction of novel SiX_2 (X = S, Se) monolayer semiconductors by density functional theory. *Phys. E Phys. E Low Dimens. Syst. Nanostruct.* **2019**, *114*, 113581. [CrossRef]
34. Kresse, G.; Furthmüller, J. Efficiency of ab-initio total energy calculations for metals and semiconductors using a plane-wave basis set. *Comput. Mater. Sci.* **1996**, *6*, 15–50. [CrossRef]
35. Kresse, G.; Furthmüller, J. Efficient iterative schemes for ab initio total energy calculations using a plane-wave basis set. *Phys. Rev. B* **1996**, *54*, 11169. [CrossRef]
36. Perdew, J.P.; Burke, K.; Ernzerhof, M. Generalized Gradient Approximation Made Simple. *Phys. Rev. Lett.* **1996**, *77*, 3865–3868. [CrossRef]
37. Kresse, G.; Joubert, D. From ultrasoft pseudopotentials to the projector augmented-wave method. *Phys. Rev. B* **1999**, *59*, 1758–1775. [CrossRef]
38. Heyd, J.; Scuseria, G.E.; Ernzerhof, M. Hybrid functionals based on a screened Coulomb potential. *J. Chem. Phys.* **2003**, *118*, 8207–8215. [CrossRef]

39. Ambrosetti, A.; Ferri, N.; DiStasio, R.A., Jr.; Tkatchenko, A. Wavelike charge density fluctuations and van der Waals interactions at the nanoscale. *Science* **2016**, *351*, 1171–1176. [CrossRef] [PubMed]
40. Chadi, D.J. Special points for Brillouin-zone integrations. *Phys. Rev. B* **1977**, *16*, 1746–1747. [CrossRef]
41. Rasmussen, F.A.; Thygesen, K.S. Computational 2D Materials Database: Electronic Structure of Transition-Metal Dichalcogenides and Oxides. *J. Phys. Chem. C* **2015**, *119*, 13169–13183. [CrossRef]
42. Yun, W.S.; Han, S.W.; Hong, S.C.; Kim, I.G.; Lee, J.D. Thickness and strain effects on electronic structures of transition metal dichalcogenides: 2H-MX_2 semiconductors (M=Mo, W;X=S, Se, Te). *Phys. Rev. B* **2012**, *85*, 033305. [CrossRef]
43. Lu, N.; Guo, H.; Zhuo, Z.; Wang, L.; Wu, X.; Zeng, X.C. Twisted MX_2/MoS_2 heterobilayers: Effect of van der Waals interaction on the electronic structure. *Nanoscale* **2017**, *9*, 19131–19138. [CrossRef] [PubMed]
44. Ding, Y.; Wang, Y.; Ni, J.; Shi, L.; Shi, S.; Tang, W. First principles study of structural, vibrational and electronic properties of graphene-like MX_2 (M=Mo, Nb, W, Ta; X=S, Se, Te) monolayers. *Phys. B Condens. Matter* **2011**, *406*, 2254–2260. [CrossRef]
45. Tsao, H.-W.; Kaun, C.-C.; Su, Y.-H. Decorating a WSe_2 monolayer with Au nanoparticles: A study combined first-principles calculation with material genome approach. *Surf. Coatings Technol.* **2020**, *388*, 125563. [CrossRef]
46. Yang, F.; Han, J.; Zhang, L.; Tang, X.; Zhuo, Z.; Tao, Y.; Cao, X.; Dai, Y. Adjustable electronic and optical properties of BlueP/MoS_2 van der Waals heterostructure by external strain: A First-principles study. *Nanotechnology* **2020**, *31*, 375706. [CrossRef]
47. Tang, Y.; Liu, M.; Zhou, Y.; Ren, C.; Zhong, X.; Wang, J. First-principles predication of facet-dependent electronic and optical properties in InSe/GaAs heterostructure with potential in solar energy utilization. *J. Alloys Compd.* **2020**, *842*, 155901. [CrossRef]
48. Hu, L.; Yi, W.; Rao, T.; Tang, J.; Hu, C.; Yin, H.; Hao, H.; Zhang, L.; Li, C.; Li, T. Two-dimensional type-II g-C_3N_4/SiP-GaS heterojunctions as water splitting photocatalysts: First-principles predictions. *Phys. Chem. Chem. Phys.* **2020**, *22*, 15649–15657. [CrossRef]
49. Zhang, J.; Ren, F.; Deng, M.; Wang, Y. Enhanced visible-light photocatalytic activity of a g-C_3N_4/$BiVO_4$ nanocomposite: A first-principles study. *Phys. Chem. Chem. Phys.* **2015**, *17*, 10218–10226. [CrossRef]
50. Wang, Z.; Zhang, Y.; Wei, X.; Guo, T.; Fan, J.; Ni, L.; Weng, Y.; Zha, Z.; Liu, J.; Tian, Y.; et al. Type-II tunable SiC/InSe heterostructures under an electric field and biaxial strain. *Phys. Chem. Chem. Phys.* **2020**, *22*, 9647–9655. [CrossRef]
51. Li, X.; Dai, Y.; Ma, Y.; Liu, Q.; Huang, B. Intriguing electronic properties of two-dimensional MoS_2/TM_2CO_2 (TM = Ti, Zr, or Hf) hetero-bilayers: Type-II semiconductors with tunable band gaps. *Nanotechnology* **2015**, *26*, 135703. [CrossRef] [PubMed]
52. Li, J.; Zhang, S.; Wang, Y.; Duan, H.M.; Long, M. First-Principles Study of Strain Modulation in S_3P_2/Black Phosphorene vdW Heterostructured Nanosheets for Flexible Electronics. *ACS Appl. Nano Mater.* **2020**, *3*, 4407–4417. [CrossRef]
53. Qu, L.-H.; Deng, Z.-Y.; Yu, J.; Lu, X.-K.; Zhong, C.-G.; Zhou, P.-X.; Lu, T.-S.; Zhang, J.-M.; Fu, X.-L. Mechanical and electronic properties of graphitic carbon nitride (g-C_3N_4) under biaxial strain. *Vacuum* **2020**, *176*, 109358. [CrossRef]
54. Zhang, Z.; Huang, B.; Qian, Q.; Gao, Z.; Tang, X.; Li, B. Strain-tunable III-nitride/ZnO heterostructures for photocatalytic water-splitting: A hybrid functional calculation. *APL Mater.* **2020**, *8*, 041114. [CrossRef]
55. Yang, Y.; Yang, Y.; Xiao, Y.; Zhao, Y.; Luo, D.; Zheng, Z.; Huang, L. Tunable electronic structure of graphdiyne/MoS_2 van der Waals heterostructure. *Mater. Lett.* **2018**, *228*, 289–292. [CrossRef]
56. Caglayan, R.; Mogulkoc, Y.; Alkan, B. First principles study on optoelectronic properties of energetically stable Si/InS van der Waals heterobilayers. *J. Mater. Sci.* **2020**, *55*, 15199–15212. [CrossRef]

Publisher's Note: MDPI stays neutral with regard to jurisdictional claims in published maps and institutional affiliations.

© 2020 by the authors. Licensee MDPI, Basel, Switzerland. This article is an open access article distributed under the terms and conditions of the Creative Commons Attribution (CC BY) license (http://creativecommons.org/licenses/by/4.0/).